Experimental investigation of the kinetics of Ostwald ripening of quartz in silicic melts

Article *in* Contributions to Mineralogy and Petrology · December 2001

DOI: 10.1007/s004100100296

CITATIONS
51

READS
149

3 authors:

Hugues Cabane
Ezus SA
24 PUBLICATIONS **200** CITATIONS
SEE PROFILE

Didier Laporte
Université Clermont Auvergne
91 PUBLICATIONS **2,454** CITATIONS
SEE PROFILE

Ariel Provost
Université Clermont Auvergne
78 PUBLICATIONS **2,907** CITATIONS
SEE PROFILE

Contrib Mineral Petrol (2001) 142: 361–373
DOI 10.1007/s004100100296

Hugues Cabane · Didier Laporte · Ariel Provost

Experimental investigation of the kinetics of Ostwald ripening of quartz in silicic melts

Received: 24 October 2000 / Accepted: 21 June 2001 / Published online: 21 August 2001

Abstract To characterise the kinetics of Ostwald ripening of quartz, we conducted four series of experiments in systems consisting of quartz, with an initial grain size of ≈1.3 to 6 μm, in equilibrium with hydrous silicic liquids. Two series were performed with a haplogranitic liquid containing 6.5 wt% H_2O at 900 °C and 1 GPa. The third series was made in the quartz–anorthite system at water saturation, 900 °C, and 1 GPa. The last series was made in the quartz–albite system at water saturation, 800 °C, and 0.2 GPa. In all series, we observed a relatively small but systematic increase of the mean grain size of quartz, $\bar{d}$, with increasing run duration, t. The largest increase was in the quartz–anorthite system: $\bar{d}$ increased by a factor of 4.3 after 326 h; the smallest increase was measured in the quartz–albite system: $\bar{d}$ increased by a factor of only ≈1.6 after 1,173 h. The experimental data yield very good linear fits in both ln t vs ln$\bar{d}$ and ln t vs $\bar{d}$ diagrams. The slopes in the ln t vs ln$\bar{d}$ diagrams, between 1/5 and 1/7, are, however, much smaller than the value of 1/3 predicted by the Lifshitz–Slyozov–Wagner theory for diffusion-controlled Ostwald ripening. A possible explanation for this discrepancy is that the diffusion-controlled regime in our experiments is only attained after a transient regime lasting from 20 h in series III to 100 h in series IV. A more straightforward explanation of the experimental results is that the rate-limiting mechanism for Ostwald ripening is quartz growth by surface nucleation not diffusion in the silicic liquid. Finally, we extrapolated our data to geological time scales to evaluate the importance of Ostwald ripening in natural quartz-bearing magmatic systems: (1) quartz cannot coarsen measurably by Ostwald ripening over reasonable time scales if the initial grain size is ≈1 mm or more; and (2) Ostwald ripening may be very active at the end of nucleation events and result in the consumption of a significant proportion of crystalline nuclei.

H. Cabane (✉) · D. Laporte · A. Provost
Laboratoire Magmas et Volcans, CNRS et Université Blaise Pascal, Observatoire de Physique du Globe, 5 rue Kessler, 63038 Clermont-Ferrand cedex, France
E-mail: cabane@opgc.univ-bpclermont.fr

Editotial responsibility: T.L. Grove

Introduction

The coarsening of solid particles in a liquid phase is known as Ostwald ripening, from the name of the chemist W. Ostwald who first observed this process (Ostwald 1901). The driving force for Ostwald ripening is the minimisation of the total interfacial energy of the system by dissolution of the smaller grains and growth of the larger ones. It results in an increase of the mean grain size and a decrease of the number of grains per unit volume. Studying the kinetics of Ostwald ripening of silicates in magmas is of major interest because the size of crystals controls the dynamics of many magmatic processes such as crystal settling or the segregation of partial melts. The settling velocity of crystals in a magma chamber or the permeability of a partially molten rock are indeed proportional to the square of grain size (e.g. Turcotte and Schubert 1982). Thus, Ostwald ripening could have important implications for magmatic processes provided its efficiency over the duration of these processes can be proved.

Ostwald ripening involves dissolution of matter from the small grains, transport by diffusion in the liquid phase, and precipitation on the large grains: so the kinetics of Ostwald ripening can be limited either by the diffusion rate or by the rate of interface reactions. Theoretical studies of the kinetics of Ostwald ripening have first been conducted for very small volume fractions of the coarsening phase (Lifshitz and Slyozov 1961; Wagner 1961). In the resulting model, called LSW, the grains are spherical, a quasi-stationary regime is assumed for diffusion, and the reaction kinetics at the interface is assumed to be linearly related to the supersaturation (continuous growth). LSW model predicts that:

1. The shape of the crystal size distribution, when normalised to the mean size, becomes stationary; the maximum grain size is 2 times the mean grain size for interface-controlled Ostwald ripening, 1.5 times the mean grain size for diffusion-controlled Ostwald ripening.
2. The mean size obeys the following law:

$$\bar{d} = \bar{d}_0 \left(1 + \frac{t}{\tau_p}\right)^{1/n} \quad (1)$$

where $\bar{d}$ is the mean grain size (or diameter), $\bar{d}_0$ is the initial mean grain size [$\bar{d}_0 = \bar{d}(t = 0)$], t is time and τ_p is a time constant depending on the interfacial energy per unit area, the initial mean grain size to the power of n, and either the diffusion coefficient in the liquid or the constant of reaction at the interface (for diffusion-controlled and interface-controlled ripening, respectively). The exponent n is 2 for interface-controlled Ostwald ripening and 3 for diffusion-controlled Ostwald ripening. Because τ_p is proportional to $\bar{d}_0^n$, Eq. (1) may be written

$$\bar{d}^n - \bar{d}_0^n = k_p t$$

where the ripening rate $k_p = \bar{d}_0^n / \tau_p$ does not depend on the initial mean grain size.

LSW theory has been extended to the case of larger fractions of solid ϕ (Ardell 1972; Brailsford and Wynblatt 1979; Marqusee and Ross 1984; Voorhees 1985): the value of exponent n is unchanged but τ_p decreases with increasing ϕ and the maximum normalised grain size $d_{\max}/\bar{d}$ increases with increasing ϕ (but remains lower than 2 in diffusion-controlled Ostwald ripening). The effect of grain shape was studied by De Hoff (1984, 1991) who showed that the value of n is not affected if the grains are not spherical. For the diffusion-controlled case he developed a model taking into account the interactions between neighbouring particles (De Hoff 1991); in this model the maximum normalised grain size is two times the mean grain size as in the interface-controlled model of Wagner (1961).

There is a good agreement between the experimental data in the materials science literature and the theoretical predictions (e.g. Kang and Yoon 1978; Kang and Yoon 1982; Fang et al. 1991). In particular, an exponent $n \approx 3$ as predicted for diffusion-controlled ripening is obtained over a wide range of liquid fractions and values of n approaching 2 are only observed for solid fractions $\phi > 95\%$vol (Kang and Yoon 1978).

There are many studies devoted to the grain growth of silicates in solid rocks (e.g. Tullis and Yund 1982; Karato 1989; Dresen et al. 1996), but comparatively very few studies on the kinetics of Ostwald ripening in partially molten rocks. Jurewicz and Watson (1985) and Laporte (1994) made measurements of dihedral angles at the junction of quartz or feldspars with a granitic melt and reported the evolution of the mean grain size with time; Park and Hanson (1999) studied the Ostwald ripening rates of forsterite in a haplobasaltic melt. In all cases it was not possible to determine accurately the kind of kinetics involved, especially the value of n. Ikeda and Nakashima (1999) performed coarsening experiments of pyroxene in liquid under static and rolling conditions. They found an exponent value of 7 for n that disagrees with theoretical works and that they did not explain. Because of the very few experimental data available for magmatic systems, we started a programme aimed at measuring the rate of Ostwald ripening for major silicate species. In this paper, we present the results for quartz in equilibrium with silicic melts.

Experimental and analytical techniques

Overview

We performed four series of experiments to measure the rate of Ostwald ripening for quartz in a silicic liquid at 900 °C and 1 GPa, and 800 °C and 0.2 GPa. In series I (runs QG1a to QG7a; Table 1) and II (runs QG1b to QG7b), the starting composition was a mixture of quartz and a synthetic granitic glass containing 6.5 wt% dissolved water (GminH); the weight percentage of quartz was 50 in series I and 73 in series II. The starting mixture was loaded into platinum containers (2-mm outer diameter) that were subsequently stored at 120 °C for 1 h before welding to remove the water adsorbed on the powder. Experimental series I and II were performed in a piston-cylinder apparatus at 900 °C and 1 GPa with durations ranging from 1 to 519 h (Table 1). In series III (runs QAn6, 7, 20, 21a, 23c, 24 and 25) and IV (runs QAb1 to QAb5), the experiments were made in the systems quartz–anorthite–H_2O and quartz–albite–H_2O, respectively, under water-saturated conditions. The starting composition was 90 wt% quartz and 10 wt% anorthite in series III, and 72 wt% quartz, 28 wt% albite in series IV. The starting mixture was loaded into platinum containers (2- and 3-mm outer diameter in series III and IV, respectively) along with de-ionised water; because a large volume percentage of bubbles would have made the textural analysis difficult, the amount of added water was just slightly larger than the amount required to saturate the system at the P–T conditions of the experiment. The bottom half of the platinum capsules was immersed into water during arc welding to minimise water loss. Experiments of series III were made in a piston-cylinder apparatus at 900 °C and 1 GPa, and lasted from 29 min to 327 h (Table 1). Experiments of series IV were conducted in an externally-heated pressure vessel at 800 °C and 0.2 GPa with duration ranging from 57 to 1,173 h.

Starting materials

Quartz

We used coarse fragments of natural, optically-clear quartz crystals cleaned in HNO_3 and HCl, and rinsed in

Table 1 Summary of run information and grain size statistics. The starting materials are, in wt%: 50% glass GminH + 50% quartz for series I (runs QG1a to QG7a), 27% glass GminH + 73% quartz for series II (runs QG1b to QG7b), 10% anorthite + 90% quartz for series III (runs labelled QAn), 28% albite + 72% quartz for series IV (runs QAb1 to QAb5). Glass GminH in series I and II contains 6.5% H_2O; experiments in series III and IV were water-saturated. Experimental conditions are 1 GPa, 900 °C for series I, II, III, and 0.2 GPa, 800 °C for series IV. Samples QAn20, 21a, 23c, 24 and 25 are taken from Laporte's (1994) study on the wetting behaviour of silicic melts. *n.a.*: not analysed

	Duration (h)	Quartz fraction[a] (vol%)	$\bar{d}_{2-D}$[b] (μm)	$\bar{d}_{3-D}$[c] (μm)	$d_{max}/\bar{d}$[d]	$\bar{C}$[e]
QG1a	126.3	46 (5)	6.2 (0.4)	5.9	3.2	0.77
QG2a	6	42 (5)	4.3 (0.3)	4.3	5.8	0.66
QG3a	519.47	41 (4)	7.9 (0.5)	8.2	3.2	0.76
QG4a	24	46 (5)	5.0 (0.3)	4.9	4.6	0.72
QG5a	1	47 (7)	3.1 (0.3)	2.8	7.7	0.61
QG6a	66	42 (5)	6.0 (0.3)	6.3	3.1	0.73
QG7a	200	45 (5)	6.4 (0.4)	6.4	2.9	0.76
QG1b	126.3	71 (6)	5.2 (0.3)	5.2	4.0	0.72
QG2b	6	68 (6)	3.5 (0.2)	3.3	5.3	0.68
QG4b	24	70 (6)	4.3 (0.3)	4.0	6.2	0.72
QG5b	1	74 (6)	2.5 (0.2)	2.4	4	0.62
QG6b	66	65 (5)	5.0 (0.3)	4.7	3.8	0.72
QG7b	200	65 (6)	5.7 (0.3)	5.4	3.6	0.75
QAn25	0.48	n.a.	5.6 (0.4)	5.7	n.a.	0.61
QAn24	2.4	n.a.	7.8 (0.5)	7.9	n.a.	0.75
QAn20	24	66 (4)	13.8 (0.6)	15.3	2.5	0.73
QAn23c	153	62 (5)	18.2 (0.9)	20.2	2.5	0.74
QAn21a	327	61 (4)	20.3 (0.9)	24.3	2.3	0.75
QAn6	66	65 (5)	15.5 (0.7)	16.4	2.7	0.70
QAn7	200	66 (4)	17.9 (0.7)	18	3.5	0.72
QAb1	165.85	51 (6)	2.8 (0.2)	3.1	4.4	0.64
QAb2	257.13	56 (6)	2.9 (0.2)	3.3	5.2	0.65
QAb3	1172.95	54 (7)	3.7 (0.3)	4.1	5.4	0.64
QAb4	56.67	55 (6)	2.4 (0.1)	2.6	4.2	0.66
QAb5	568.72	55 (6)	3.2 (0.2)	3.6	5.5	0.62

[a]The volume fraction of quartz is supposed to be equal to the surface fraction of quartz in plane sections. The error (in parentheses) is equal to half the difference between a maximum estimate of surface fraction (after one morphological dilation of the binary images) and a minimum estimate of surface fraction (after one morphological erosion of the binary images)
[b]$\bar{d}_{2-D}$ is the measured 2-D mean grain size (the error is given in parentheses)
[c]$\bar{d}_{3-D}$ is the estimated 3-D mean grain size (see the text for further explanation)
[d]$d_{max}/\bar{d}$ is the maximum 2-D grain size divided by the 2-D mean grain size
[e]$\bar{C}$ is the mean compactness of the population of grains measured in a sample (typical error: ±0.03)

distilled water. For series I to III, the quartz was ground in acetone, sieved with a 20-μm mesh and finally fired at 800 °C to produce a well-sorted powder of angular fragments. From grain size analysis in the shortest experiments of series I, II and III, the mean grain size of quartz in the starting powder was estimated to be 2.5 μm for series I and II, 5 μm for series III; despite sieving with a 20-μm mesh, a few grains with a greatest length of 40–50 μm were still present.

Because the kinetics of Ostwald ripening was anticipated to be slower at 800 °C and 0.2 GPa, we used a much finer quartz powder in series IV: a coarse powder of quartz was ground in a micronising mill for 25 min in ethanol. The alcoholic suspension was let 60 h to ensure the separation of quartz from the ethanol by settling; the quartz powder was finally dried and fired at 800 °C. The maximum size was < 10 μm and the mean grain size estimated from extrapolation of our data for a short time (1 h, for instance) was about 1 μm.

Plagioclases

Fine powders of synthetic anorthite (< 20 μm) and Amelia albite were used in starting compositions III and IV, respectively. The reader is referred to Laporte (1994) for technical information on the anorthite. A fine powder of Amelia albite with a maximum size of < 10 μm was prepared using the same procedure as for series IV quartz.

Granitic glass

Hydrous granitic glass GminH was prepared by water saturation of haplogranitic glass Gmin (Table 2) in an externally-heated pressure vessel at 760 °C and 200 MPa for 6 days. Samples of 260 mg of glass Gmin were loaded along with 30 mg distilled water into a gold capsule. The capsule was cooled with liquid nitrogen during arc-welding to avoid water vaporisation. After the experiment, the H_2O-saturated glass was ground to less than 20 μm. A loss-on-ignition test indicated a water content of 6.5 wt% for GminH.

Apparatus

Experimental series I to III were conducted in a 3/4″ piston-cylinder apparatus using NaCl-soft glass-graphite-crushable MgO assemblies. The platinum capsules were placed vertically, by groups of three, at the hot spot

Table 2 Average compositions of glasses in wt%. Analytical conditions for electron microprobe are 15 kV, 5 nA, 10 s, and beam size is 5×5 μm. Oxide concentrations are given after normalisation to 100 wt% of the totals of the major elements; analytical totals are shown for information (last column). Standard deviations are given in parentheses. The number of analyses is given in parentheses after the run number

	SiO_2	Al_2O_3	Na_2O[a]	K_2O	CaO	Total
Gmin[b]	76.92	13.27	4.73	5.08	–	100.00
QG1a (6)	78.29 (0.26)	12.99 (0.25)	3.86 (0.11)	4.86 (0.11)	–	93.86
QG2a (7)	79.14 (0.30)	12.60 (0.15)	3.41 (0.17)	4.84 (0.12)	–	94.05
QG3a (5)	78.00 (0.23)	13.23 (0.14)	3.73 (0.03)	5.04 (0.13)	–	93.83
QG4a (5)	78.72 (0.26)	12.82 (0.18)	3.50 (0.06)	4.95 (0.10)	–	93.91
QG6a (6)	78.43 (0.11)	12.85 (0.08)	3.83 (0.13)	4.89 (0.16)	–	92.00
QG7a (6)	77.96 (0.27)	13.13 (0.13)	4.00 (0.16)	4.91 (0.15)	–	95.08
QAn24 (5)	80.00 (0.15)	12.78 (0.24)	–	–	7.22 (0.15)	86.42
QAn6 (6)	80.35 (0.28)	12.42 (0.27)	–	–	7.22 (0.17)	85.64
QAn7 (6)	79.54 (0.30)	13.00 (0.22)	–	–	7.46 (0.19)	88.69
QAb1[c] (5)	83.72 (0.58)	10.88 (0.54)	4.99 (0.10)	0.29 (0.11)	0.12 (0.08)	91.14
QAb2[c] (5)	83.68 (0.35)	11.14 (0.21)	4.52 (0.20)	0.50 (0.29)	0.16 (0.04)	90.33
QAb3[c] (6)	83.38 (0.17)	11.10 (0.12)	5.15 (0.16)	0.23 (0.08)	0.14 (0.03)	90.11
QAb4[c] (4)	84.75 (0.87)	9.97 (0.72)	4.55 (0.24)	0.53 (0.13)	0.20 (0.07)	91.36
QAb5[c] (4)	83.90 (0.25)	11.00 (0.21)	4.62 (0.20)	0.36 (0.17)	0.12 (0.03)	91.17

[a]Sodium loss is estimated to ≈15% relative
[b]Calculated from weights of oxides and carbonates (Laporte 1994)
[c]Glasses in series IV contain in addition ≈0.2wt% FeO and ≈0.2 wt% MgO

of the graphite furnace. The techniques used to heat and to pressurise the assemblies and to monitor the temperature were similar to those described in Laporte (1994). Series IV was performed in an externally-heated pressure vessel made of a nickel-based superalloy (Nimonic 105). The platinum capsules were first pressurised (using nitrogen) and then heated to 800 °C in about 60 to 90 min. Temperature was controlled with a Pt100/Pt90Rh10 thermocouple calibrated against the melting point of NaCl. Pressure was measured by a pressure transducer precise to <1 MPa. The experiments were quenched by lifting the furnace and cooling the pressure vessel with compressed air; the resulting quench rate was 3–4 °C/s.

Analytical techniques

After an experiment, the platinum capsules were opened and some fragments of the samples were mounted in epoxy, ground and polished with 1.0 and 0.3 μm alumina grit. Compositions of experimental glasses were determined with a Cameca SX100 electron microprobe, at 15 kV, 5 nA and with counting times of 10 s. We used a beam size of 5×5 μm. For hydrous granitic glasses, this beam size is not large enough to reduce sodium loss to a negligible level (Laporte 1994): sodium loss is ≈15% relative for a 5×5 μm beam size. The compositions of experimental glasses are given in Table 2.

For textural analysis, the polished samples were observed with a Cambridge Stereoscan S360 scanning electron microscope (SEM). For each sample, four to six back-scattered electron images were stored with a resolution of 768×574 pixels; magnifications ranging from 650 to 2,000 were used depending on grain size, so that the total number of quartz grains available for shape and size analysis was larger than 500 in each sample.

Stereology

Binary images were generated from the back-scattered electron images using the image analysis software Micromorph (Centre de morphologie mathématique, Ecole des Mines de Paris 1996). The size (diameter of the disc with the same area) and the Ferret diameters (length of the orthogonal projections of the grain on the edges of the image) were measured for each grain. To obtain 2-D crystal size distributions, we corrected for the edge effect, following a method from Lantuéjoul (1980):

$$f_{2D}(i) = \frac{\sum_{j, d_i \le d(j) < d_{i+1}} \frac{1}{(L-l(j))(W-w(j))}}{\sum_j \frac{1}{(L-l(j))(W-w(j))}}$$

where $f_{2D}(i)$ is the frequency of grain sections whose size is included into $[d_i, d_{i+1}]$, $d(j)$ is the size of the jth grain section, $l(j)$ and $w(j)$ are the Ferret diameters of the jth grain section, L and W are the image length and width. The number per unit area of grain sections whose size is within $[d_i, d_{i+1}]$, $n_a(i)$, is related to $f_{2D}(i)$ as follows:

$$n_a(i) = f_{2D}(i) \sum_j \frac{1}{(L - l(j))(W - w(j))}$$

We used a method from Saltikov (1967) to estimate the number of grains per unit volume and the mean 3-D diameters. Because the quartz grains have equant shapes in our experiments (Fig. 1), we assumed a spherical shape for the grains. If the d_i are geometrically spaced ($d_{i+1} = a\ d_i$), and if there are N bins of increasing sizes ($a > 1$), the following expressions give the number of grains per unit volume, n_v, in each 3-D size bin:

$$n_v(N) = \frac{n_a(N)}{H_N P_N}$$

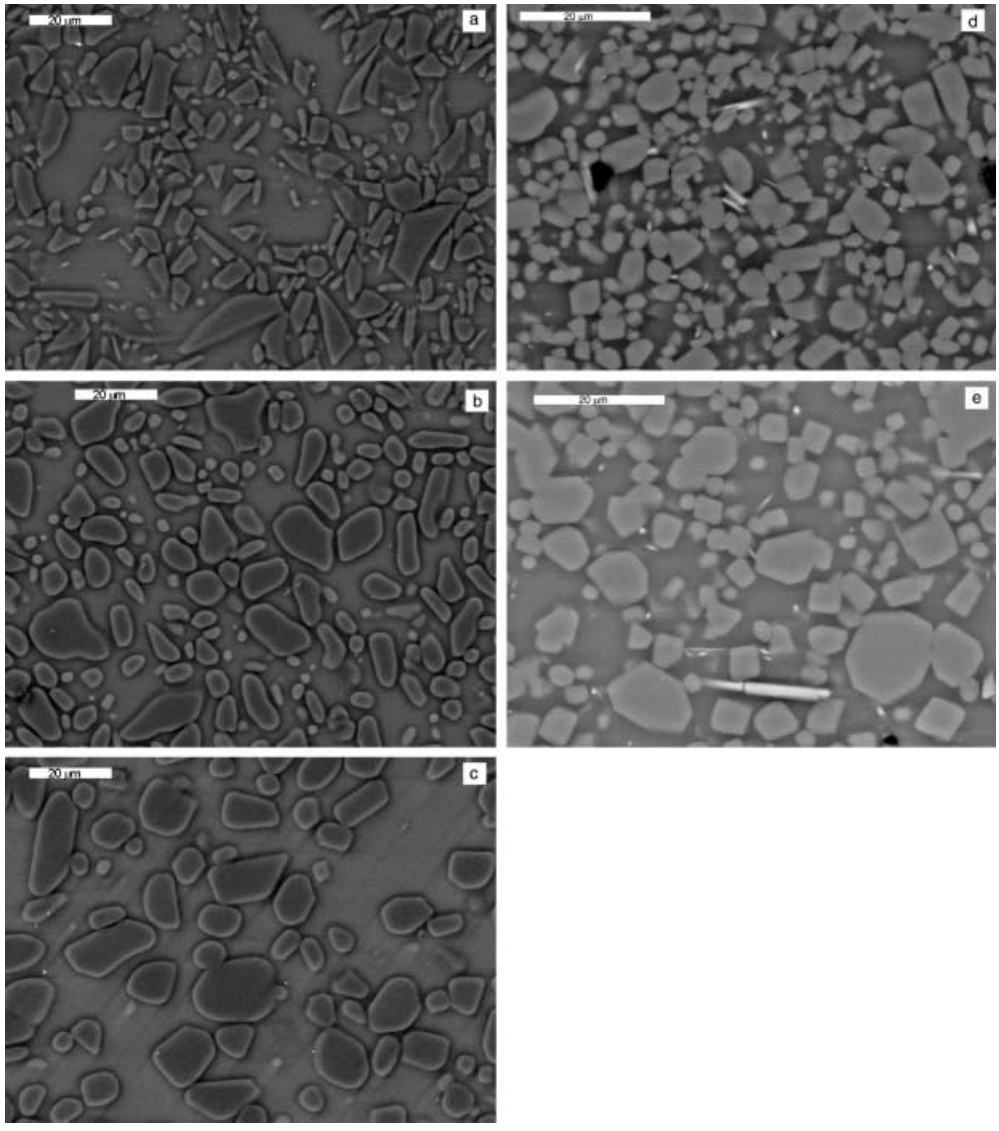

Fig. 1a–e Back-scattered electron images of experimental samples from series I (**a** 1 h, **b** 24 h, **c** 519 h) and from series IV (**d** 57 h, **e** 1,173 h)

$$n_v(N-i) = \frac{n_a(N-i) - \sum_{j=N-i+1}^{N} n_v(j) H_j P_{2N-j-i}}{H_{N-i} P_N}$$

where H_i is the mean projected height defined as the distance between tangent planes averaged over all orientations of the particle (for a sphere, H_i is equal to the diameter of the spheres in the ith bin); P_i is the probability for a sphere in the jth bin to have a section in the (j–i)th bin: it does not depend on j because the bins are geometrically spaced and $P_i = \sqrt{1 - a^{-2(N-i+1)}} - \sqrt{1 - a^{-2(N-i)}}$. The mean 3-D diameter is then easily computed from the n_v. Although most of the corrected results are satisfying, this method leads sometimes to overcorrected values ($n_v < 0$) for the small size bins, and increases the dispersion data. Thus our raw, model-independent 2-D data are also presented.

Texture characterisation

To quantify the shape of the grains we measured the compactness of the grains defined as follows:

$$C = \frac{4\pi S}{p^2}$$

where S is the area of the section of the grain and p its perimeter. C ranges from 0 to 1 and is maximum for a disc. C has been computed for each particle (except the smallest ones, see below) and the average value $\bar{C}$ is reported in Table 1; the standard error is $\sigma_C/\sqrt{N_m}$ where σ_C is the standard deviation of the compactness and N_m is the number of grains measured. Because of the absence of an univocal definition of the perimeter of a particle in discrete geometry, C can significantly depend on the definition chosen to estimate p, especially for small particles. Therefore, the shape parameter was

computed only for particles with more than 100 pixels. Yet, C is still slightly affected by the size of the particles. To minimise this artefact, we controlled that the mean number of pixels for the diameter of a grain is approximately the same for all the images we analysed.

Experimental results

Petrology

Paragenesis

In series I and II, the synthetic glass GminH is near chemical equilibrium with quartz at the P–T conditions of the experiments: at 900 °C and 1 GPa, glass GminH only dissolved ≈5 wt% of quartz and precipitates trace amounts of a K_2O-rich alkali feldspar (Laporte 1994).

For series III and IV, a melting reaction involving H_2O, quartz, and anorthite (III) or albite (IV) occurred at the beginning of the experiments. The reaction proceeded until anorthite or albite was exhausted, the other reagents being in excess. The final paragenesis was therefore quartz, a water-saturated liquid and a free fluid phase in both cases. For series IV, some orthopyroxenes were also observed. The trace amounts of MgO and FeO in Amelia Albite are presumably responsible for that feature. We emphasise that the time scale of the melting reactions in series III and IV was very short compared with the run duration: we did not observe any residual albite or anorthite even in the shortest experiments (29 min in series III, run QAn25; 57 h in series IV, run QAb4).

Chemical evolution

To check that precipitation of quartz did not occur to a significant level in our experiments and that grain coarsening was only controlled by Ostwald ripening, we plotted the SiO_2 concentrations in liquid and the surface fraction of quartz as a function of run duration (Fig. 2a, b). The variations of SiO_2 concentrations with time are very small and hardly exceed the analytical error (±0.6 wt%). Quartz precipitation or dissolution would have given rise to a negative correlation between SiO_2 concentration in liquid and surface fraction of quartz. The analytical error on the surface fraction of quartz is large (typically ±5 vol%, Table 1). The absence of correlation between the surface fraction of quartz and SiO_2 concentration in liquid suggests, however, that no significant precipitation or dissolution of quartz occurred in our experiments.

Textures

Grain shape

The evolution of grain shape with time is qualitatively shown on BSE images for series I (Fig. 1a, c) and IV (Fig. 1d, e). For series I a spectacular change is visible from 1 to 24 h: the grain shape evolves from angular shards to smooth and rounded grains. Changes in grain shape are less obvious from 24 to 519 h, but the development of facets is noticeable. For series IV there is almost no evolution of grain shape. This can be explained by the smaller initial grain size and the long duration of all the experiments: a near equilibrium shape is probably reached even in the shortest experiment, QAb4 (57 h; Table 1).

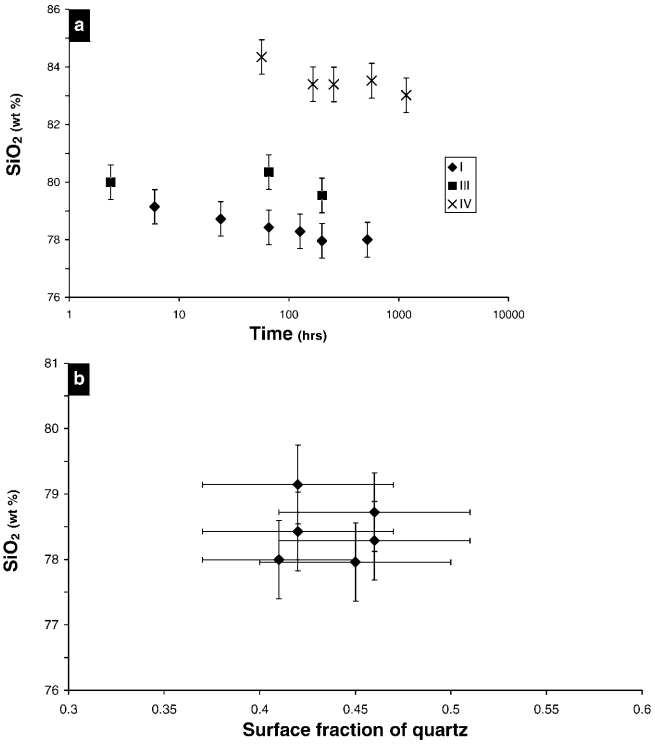

Fig. 2 **a** SiO_2 concentration (wt%) as a function of run duration in series I, III, and IV. **b** SiO_2 concentration as a function of the surface fraction of quartz in series I. Analytical error for the concentration of SiO_2 is ±0.6 wt%

The evolution of the mean compactness is reported for each series in Fig. 3. For series IV, a slight decrease of $\bar{C}$ is observed with increasing run duration. For series I to III, $\bar{C}$ increases from ≈0.61 to ≈0.75 especially within the first 2 h (series III) to 24 h (series I, II). The faster increase in series III is presumably caused by the larger water content in the melt (≈12 wt%). The evolution of $\bar{C}$ in series I to III becomes sluggish at long run durations and it reaches a plateau, corresponding on the BSE images to near equilibrium grain shapes (Fig. 1c). The value of $\bar{C}$ in the long duration experiments is clearly much larger in series I to III (≈0.75) than in series IV (≈0.64). The quartz grains in series IV are indeed faceted and show sharp edges (Fig. 1e), whereas they are more rounded in series I, II and III (Fig. 1c). The plateau values of $\bar{C}$ are indicated by the two shaded zones in Fig. 3. It is interesting to compare the measured values with the values of $\bar{C}$ computed for a suspension of hexagonal bipyramids with more or less rounded grain

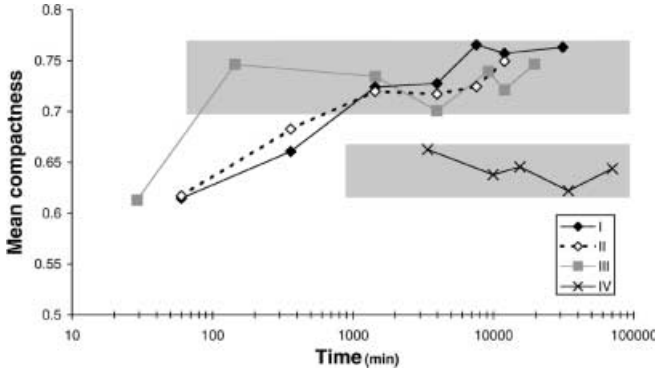

Fig. 3 Evolution with time of the mean compactness $\bar{C}$ (the error is ± 0.03). With time, grains approach an equilibrium shape and $\bar{C}$ reaches a plateau value (shaded areas) of ≈ 0.64 for series IV and ≈ 0.75 for series I–III

edges (a hexagonal bipyramid with rounded edges is the equilibrium shape of quartz in our experimental conditions; Laporte and Provost 1994). We first generated a 2-D texture by random sectioning of bipyramids with sharp edges. The polygonal sections were then rounded by a morphological opening by an isotropic structuring element of size 11 pixels (to simulate the more rounded grain shapes observed in series I, II, III) or of size 3 pixels (to simulate the grain shapes with sharp edges observed in series IV). The values of $\bar{C}$ computed for openings of size 3 and 11 are 0.63 and 0.75, respectively. Therefore, the measured values of $\bar{C}$ (≈ 0.64 in series IV; ≈ 0.75 in series I to III) are in good agreement with the values expected for a population of hexagonal bipyramids with random orientation. In addition, the equilibrium crystal shape of quartz appears to be much more rounded at 900 °C and 1 GPa (series I to III; Fig. 1c) than at 800 °C and 0.2 GPa (series IV, Fig. 1e).

Crystal size distributions

The effect of Ostwald ripening on the CSD is illustrated in Fig. 4a for three experiments of series I: 1, 24 and 519 h. With time, the frequencies (expressed as the number of grains in a histogram class divided by the total number of grains measured) of small-grain classes decrease and the frequencies of larger-grain classes increase. As a result, the CSD becomes wider, the mode is shifted towards larger grain sizes, and the maximum frequency decreases. LSW theory (Lifshitz and Slyozov 1961; Wagner 1961) predicts that, after normalisation to the mean grain size, the CSD should reach a steady-state profile with time. Successive normalised CSDs do not superimpose well for series I, II and III, as shown in Fig. 4b for series I. A possible explanation for this discrepancy may be that even in the longest experiments, the final CSD kept a memory of the initial CSD. The starting powders used in series I to III contained indeed low frequencies of relatively large grains (up to 40 or 50 μm long). Accordingly, a significant proportion of the

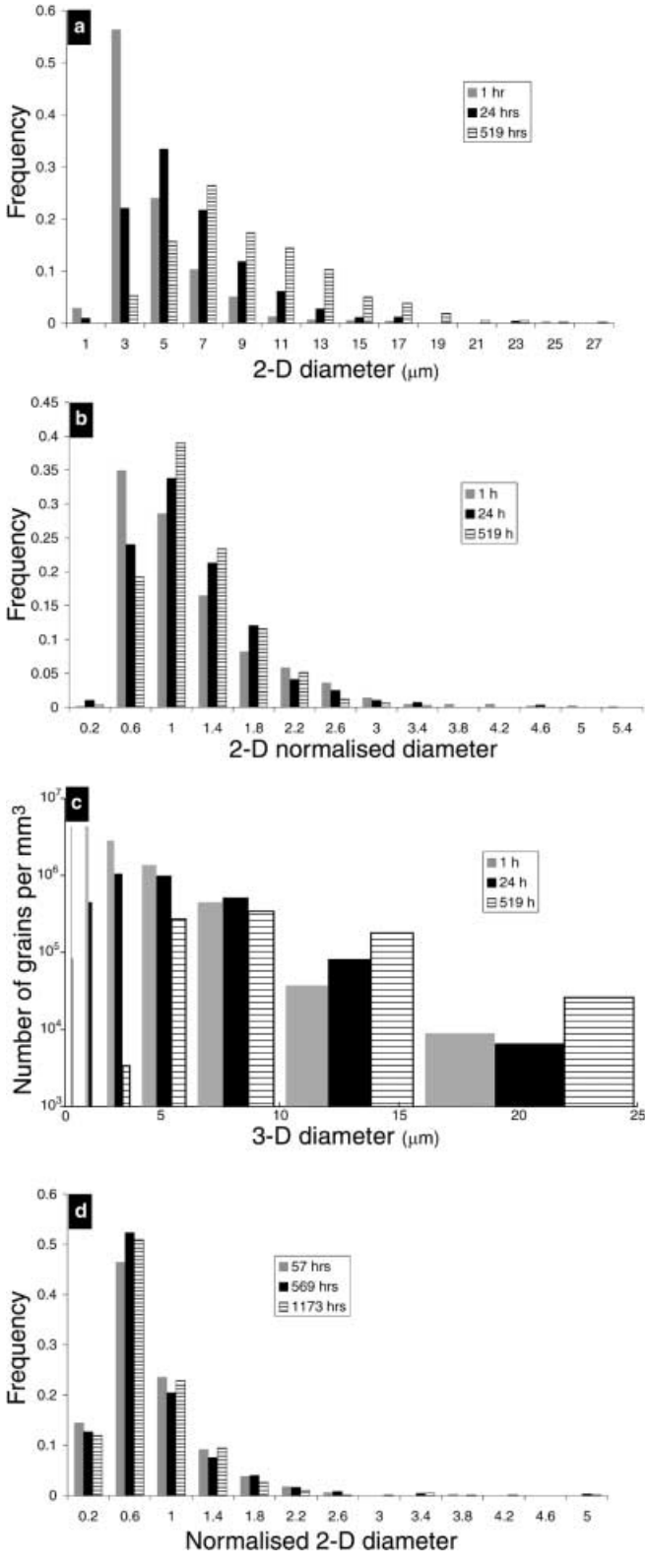

Fig. 4a–d Evolution with time of the CSD (in **a**, **b** and **d** the frequencies are the number of grains in a histogram class divided by the total number of grains measured; in **c**, the frequencies are the number of grains per mm^3 in a histogram class). **a–c** CSDs for series I at 1, 24, 519 h; in **b** the CSDs are normalised to the mean grain size. **d** Normalised CSDs for series IV at 57, 569 and 1,173 h

larger grains in the final CSDs may be inherited from the starting powder. In Fig. 4c, in which the CSDs are corrected into 3-D CSDs, the number of grains per unit volume for the largest size bin does not increase from 1 to 24 h, as expected if these grains were predominantly inherited from the starting powder.

Contrary to series I to III, series IV shows steady-state normalised CSDs (Fig. 4d). In this series, the initial CSD was presumably rapidly erased owing to the much finer starting powder. The procedure used to prepare this powder ensured indeed that no quartz grain larger than 10 μm was present. We stress, however, that the shape of the normalised CSDs in series IV is quite different from the steady-state profile calculated in theoretical works: the peak region is more or less symmetric whereas it should be negatively skewed; the maximum normalised size (≈5, Table 1) is much larger than the predicted values of 2 (interface-controlled kinetics) or 1.5 (diffusion-controlled kinetics). Thus the normalised CSD reaches a steady-state profile, which is not the one proposed in LSW theories.

Mean grain size

The mean grain size increased significantly in the four experimental series (Table 1): from 2.8 μm (1 h) to 8.2 μm (519 h) in series I; from 2.4 μm (1 h) to 5.4 μm (200 h) in series II; from 5.7 μm (29 min) to 24.3 μm (327 h) in series III; and from 2.6 μm (57 h) to 4.1 μm (1,173 h) in series IV. Very contrasted kinetics of Ostwald ripening are observed in the four series (Fig. 5). The series run at 900 °C and 1 GPa and water saturation (series III) shows the fastest kinetics. By comparison, the kinetics of Ostwald ripening in series I and II run at the same P–T conditions but with a lower water content in the liquid (6.5 versus ≈12 wt% in series III) is much slower. The slowest kinetics is observed in series IV that was run at water saturation but at lower P and T conditions (≈6.5 wt% water, 0.2 GPa and 800 °C). In Fig. 5, we plotted the data from Jurewicz and Watson (1985) for Ostwald ripening of quartz in a H_2O-poor granitic liquid (0.2 wt%) at 1 GPa, 1,000 °C. Despite the higher temperature, Ostwald ripening under these conditions was slower than in our series IV, which was run at a lower temperature (800 °C) but with a larger water content in the liquid (6.5 wt%).

Assuming that the mean grain size obeys equation 1 with $t \gg \tau_p$, each experimental slope should form a line in a $\ln \bar{d}$ versus $\ln t$ diagram with a slope equal to $1/n$. As a matter of fact, a very good linear correlation between $\ln \bar{d}$ and $\ln t$ is obtained for the four series (Fig. 5a, c). The lines for all the series are roughly parallel and correspond to values of n ranging from 5.1 to 7.2 for 2-D values, 4.7

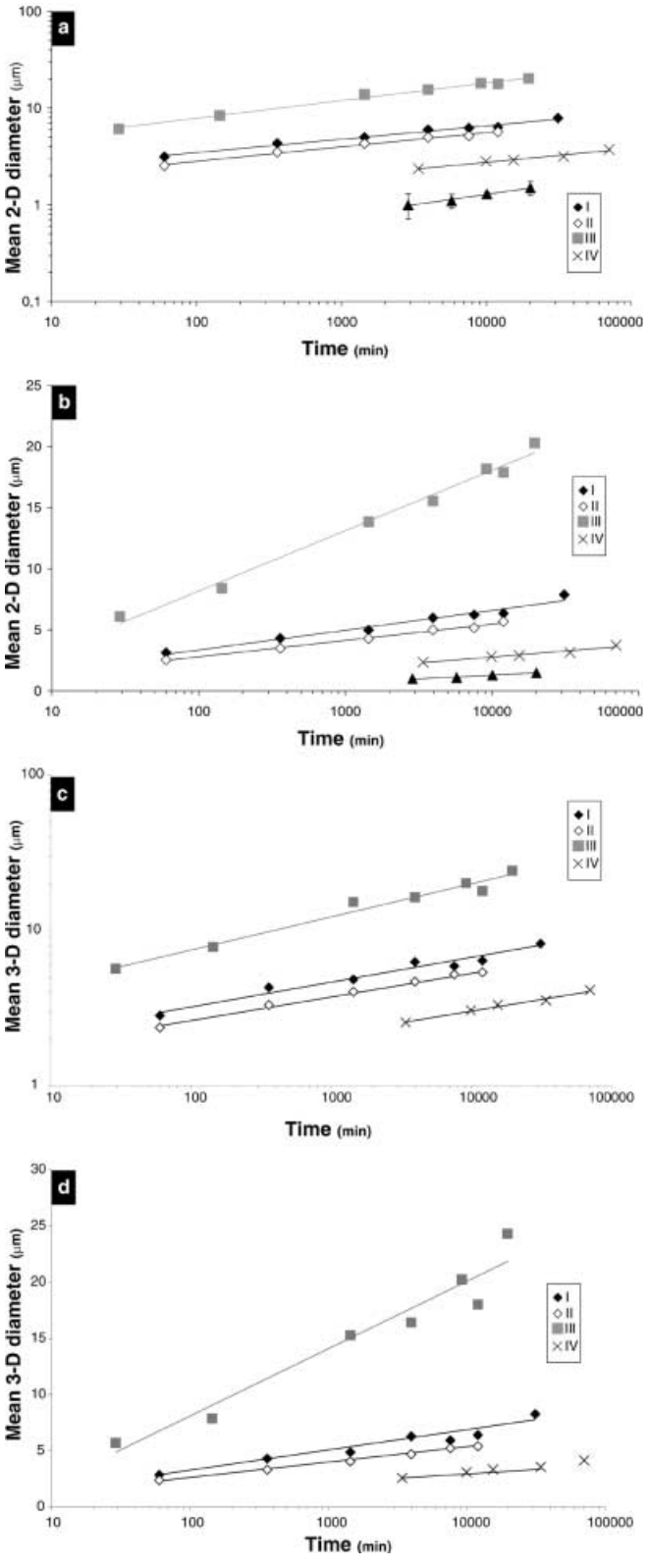

Fig. 5a–d Evolution with time of the mean grain size (**a–b** 2-D mean grain size; **c–d** 3-D mean grain size). *Full diamonds*: series I; *empty diamonds*: series II; *shaded squares*: series III; *crosses*: series IV. The *triangles* (**a–b**) are data from Jurewicz and Watson (1985; 1 GPa, 1,000 °C, 0.2 wt% water in the liquid). The data are plotted in a *ln/ln diagram*, and fitted by power laws (**a–c**), or plotted in a *half-ln diagram*, and fitted by logarithmic laws (**b–d**). *Error bars*, if not visible, are within the *symbols*

to 6.6 for 3-D values. These values of n are much larger than those predicted by LSW theory: 2 for interface-controlled kinetics, 3 for diffusion-controlled kinetics.

The very small values of the slope $1/n$ in the ln t vs ln $\bar{d}$ diagram suggest that our experimental data may as well be fitted by a logarithmic law:

$$\bar{d} = \bar{d}_0 + k_l \ln\left(1 + \frac{t}{\tau_l}\right) \quad (3)$$

where k_l, τ_l are constants, with the dimensions of a length and a time, respectively. We made the assumptions that k_l and τ_l do not depend on $\bar{d}_0$. Good linear correlations between $\bar{d}$ and ln t are obtained for series I to IV (Fig. 5b, d).

In parallel to the increase of the mean grain size, the number of grains per unit volume, N_v, decreased during Ostwald ripening. N_v was computed using the Saltikov method (see section Stereology); it decreased much in the beginning of coarsening: in series I and II for instance, it is divided by ≈3.7 during the first 24 h. The evolution of N_v with time is well fitted by a power law (Fig. 6): N_v is linearly related to the inverse of time at the power α, where α ranges from 0.41 to 0.51.

Discussion

Interpretation of experimental data

The very good linear correlations observed between ln t and ln $\bar{d}$ correspond to values for the exponent n much larger than the values predicted by LSW theory: $n \approx 5$–7 instead of $n = 2$ for interface-controlled kinetics, or $n = 3$ for diffusion-controlled kinetics. Similarly, Jurewicz and Watson's (1985) data for quartz in a dry granitic melt show a good linear correlation in a ln $\bar{d}$ versus ln t plot, but with a slope of ≈1/5 instead of 1/2 or 1/3 as predicted by LSW theory (Fig. 5a). Our data and those from Jurewicz and Watson (1985) are equally well fitted by a logarithmic law (Fig. 5b).

Two fundamentally different ways to interpret the discrepancy between our experimental results and LSW theory are discussed in the following sections.

The concept of a transient regime

For the four experimental series, reasonably good linear correlations are obtained between $\bar{d}^3$ and t if the shorter experiments are not taken into account. This point is illustrated in Fig. 7 in which the data for series I are plotted in a $\bar{d}^3$ vs t diagram. From this figure, we could conclude that, after a transient regime lasting about 50 h, a permanent regime is established, in which the kinetics of Ostwald ripening kinetics is controlled by diffusion in the liquid ($\bar{d}^3 \propto t$).

Plots of $\bar{d}^3$ vs t for series II to IV can also be interpreted in terms of a transient regime lasting ≈20 (series III) to ≈100 h (series IV) followed by a permanent, diffusion-controlled regime (Table 3). Using LSW equations, diffusion coefficients can be estimated from the slope of the linear part of the experimental trends in the $\bar{d}^3$ vs t diagram. These estimates range from 10^{-14} m^2/s in series IV to 10^{-11} m^2/s in series III and are in reasonable agreement with the diffusion coefficient for Si in a hydrous granitic liquid at 800–900 °C: ≈10^{-13} m^2/s as extrapolated from Baker's (1991) data.

Ostwald ripening controlled by surface nucleation

The exponent $n = 2$ predicted by LSW theory for interface-controlled ripening corresponds to the case where the rate-limiting mechanism is continuous growth. For continuous growth, the growth/dissolution rate at the crystal–liquid interface is proportional to supersatura-

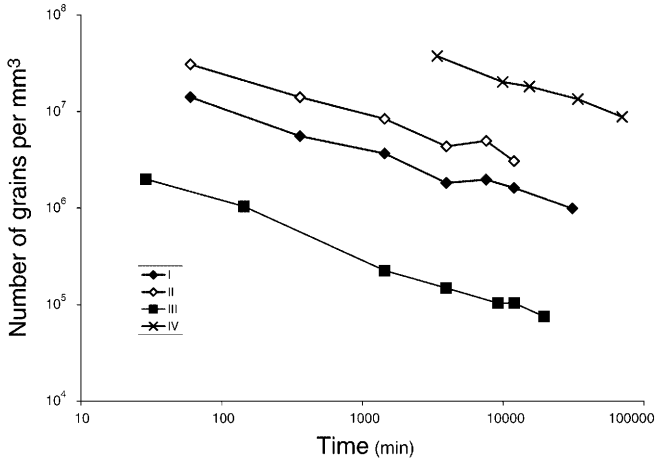

Fig. 6 Evolution of the number of grains per mm^3. *Full diamonds*: series I; *empty diamonds*: series II; *shaded squares*: series III; *crosses*: series IV

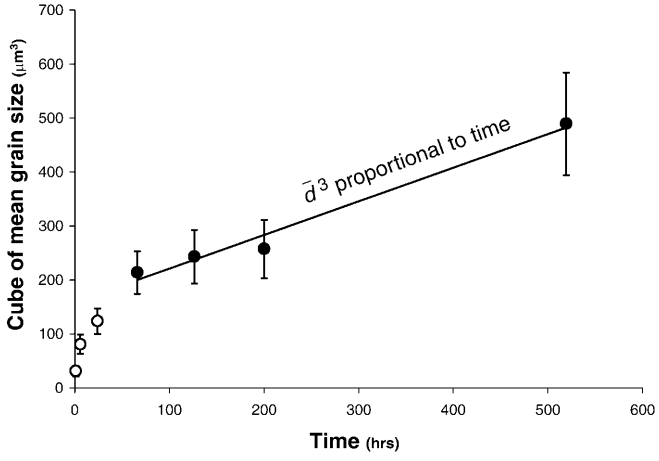

Fig. 7 Evolution of the cube of the mean grain size for series I (2-D data). The longer experiments (*full circles*) are fitted by a linear law. Short duration experiments are plotted as *empty circles*

Table 3 Parameters used to fit the experimental 3-D data using a cube root law in time following a transient regime. The time θ (h) is the estimated duration of the transient regime (Fig. 7); a (μm^3/h) is the slope of the linear part of the experimental trend in a $\bar{d}^3$ vs t plot, and D is the diffusion coefficient computed from a using the LSW equations; y_0 (μm^3) is the intersection of this line with the $\bar{d}^3$ axis at $t=0$. Parameter r is the correlation coefficient of Pearson between t and $\bar{d}^3$ in this plot and for the linear part of the experimental trend

	θ	a	D	y_0	r
I	50	0.78	3×10^{-13}	141.5	0.965
II	20	0.51	2×10^{-13}	63.3	0.959
III	20	33.4	10^{-11}	2146	0.912
IV	100	0.04	10^{-14}	23.9	0.993

Table 4 Equations used to fit the experimental data using a logarithmic law [see Eq. (3)]. Both 2-D mean grain sizes and 3-D mean grain sizes were fitted. Values of k_l and of $\bar{d}_0 - k_l \ln \tau_l$ were estimated assuming $t \gg \tau_l$; units for length and time are μm and s. Parameter r is the correlation coefficient of Pearson between ln t and $\bar{d}$

		k_l	$\bar{d}_0 - k_l \ln \tau_l$	r
I	2-D	0.7	–2.8	0.983
	3-D	0.8	–3.6	0.966
II	2-D	0.6	–2.3	0.997
	3-D	0.6	–2.4	0.997
III	2-D	2.1	–10.5	0.994
	3-D	2.6	–14.8	0.968
IV	2-D	0.4	–2.9	0.978
	3-D	0.5	–3.5	0.989

tion/undersaturation (Wagner 1961), and the crystals are expected to be more or less rounded with microscopically rough interfaces (Dowty 1980; Baronnet 1984). By comparison, the quartz crystals in our experiments have macroscopically flat, crystallographically controlled rational faces and show only a limited rounding of their edges, especially in series IV (Fig. 1c, e). Accordingly, these crystals may have grown by a layer growth mechanism (Dowty 1980): spiral growth in the presence of screw dislocations or surface nucleation in which each layer is initiated by a two-dimensional nucleus. Solomatov and Stevenson (1993) theoretically studied the kinetics of interface-controlled Ostwald ripening in the case of layer growth. They found that the mean grain size was proportional to $t^{1/3}$ for spiral growth and to ln t for growth by surface nucleation. To our knowledge, there is no layer growth mechanism yielding a power law relationship $\bar{d} \propto t^{1/n}$ with n in the range of 5–7.

Accordingly, a model of interface-controlled Ostwald ripening in which the rate-limiting mechanism is quartz growth by surface nucleation may explain both the faceted habit of quartz and the very good linear fits in the $\bar{d}$ vs ln t diagrams ($r \approx 0.98$, Table 4). In this model, a corollary of our experimental study is that the growth mechanism of quartz in hydrous silicic liquids at 800–900 °C, 0.2–1 GPa, and for small supersaturations is surface nucleation.

Arguments against diffusion-controlled Ostwald ripening

Although we lack definitive evidence, we believe that the rate-limiting process for Ostwald ripening in our experiments is quartz growth by surface nucleation, not diffusion in the liquid. The two main arguments against the diffusive model are the following:

1. The good linear correlations observed between $\bar{d}^3$ and t in the long duration experiments may be fortuitous. Indeed for any kinetic law in ln t or in $t^{1/n}$ with n large (5–7 in our data), it is always possible to find a restricted range of t over which the data can be fitted by a $t^{1/3}$ law. In fact, we could as well fit our data with a $t^{1/2}$ law (the transient regime would be just longer than in Fig. 7). The only element in keeping with diffusion-controlled Ostwald ripening is that the diffusion coefficients computed from the slope of the linear part of the $\bar{d}^3$ vs t diagrams are in reasonable agreement with the diffusion coefficient of Si in a silicic liquid at 800–900 °C.
2. The second argument against a diffusion-controlled model is based on the observation that the average distances between neighbouring grains in our systems are very small: only a few microns (Fig. 1). To compute these distances, we assumed that a sphere of volume N_v^{-1} was associated to each of the N_v grains of quartz per unit volume (each sphere contains one grain surrounded by a shell of liquid). Then the average distance between the surfaces of two neighbouring grains may be approximated by the difference $2R - \bar{d}$, where R is the radius of a sphere of volume N_v^{-1}. Using this formula, we computed average distances between 2 and 5 μm in series I–III and between 1 and 2 μm in series IV. In all series, the average distance increased with increasing run duration (because of the decrease of N_v), but the increase was less than by a factor two.

Finally, numerical computations in progress (Cabane, unpublished data) confirm that our experimental data are best simulated by a model in which the kinetics of Ostwald ripening is controlled by quartz growth by surface nucleation.

Geological implications

To estimate the effect of Ostwald ripening on the grain size of quartz in magmatic systems, we extrapolated our experimental data to geological time scales using both the cube root law and the logarithmic law in time. The extrapolated 3-D mean diameters ($\bar{d}_{3-D}$) in Tables 5 and 6 were computed using the relationships in Tables 3 and 4. The $\bar{d}_{3-D}$ extrapolated to 10,000 a or 1 Ma are very strongly dependent on which of the two kinetic laws is

Table 5 Three-dimensional mean grain sizes (μm) extrapolated from our experimental data to long times, assuming a cube root law in time (Table 3). The error as a result of extrapolation is given in parentheses

	I	II	III	IV
$\bar{d}_0$[a]	≈2.5	≈2.1	≈5	≈1
1 a	19 (1)	17 (2)	67 (6)	7 (1)
100 a	88 (6)	77 (6)	308 (28)	33 (1)
10,000 a	408 (28)	355 (26)	1,430 (132)	152 (5)
1 Ma	1,894 (130)	1,650 (125)	6,636 (611)	704 (20)

[a]Estimated initial 3-D mean grain sizes

considered: the mean grain sizes at $t = 1$ Ma, for instance, are ≈two orders of magnitude larger in the case of a cube root law in time than in the case of the logarithmic law. For the latter case, the mean grain size at $t = 1$ Ma ranges from 12 to 20 μm only for series I, II, IV (with ≈6.5 wt% H_2O in the liquid; Table 6); the kinetics is slightly faster in series III because of the larger water content in the liquid (≈12 wt%; Table 2), but still $\bar{d}_{3-D}$ is only ≈70 μm at $t = 1$ Ma. For comparison, the $\bar{d}_{3-D}$ extrapolated to 1 Ma using the $t^{1/3}$ law are 0.7 mm in series IV, ≈2 mm in series I and II, and up to ≈7 mm in series III (Table 5).

Implications for the grain size of quartz in granites and migmatites

Ostwald ripening of quartz could possibly operate in crustal protoliths during regional scale anatexis and in large granite bodies crystallising slowly in depth because of the long time scale characteristic of these contexts (typically $> 10^6$ years for crustal melting at the regional scale; Brown et al. 1995). If, over the corresponding time scales, a significant increase of the mean grain size occurs by Ostwald ripening, then the dynamics of melt segregation or of crystal settling could be greatly accelerated, as mentioned in the introduction. Granites that crystallised slowly are coarse-grained, with a grain size of the order of 1 cm. The grain size in migmatites and in high-grade metamorphic rocks is variable, but commonly in the range 0.1 mm to a few millimetres.

Series IV provides the best basis to discuss the effect of Ostwald ripening on the grain size of quartz because the experimental conditions (800 °C, 0.2 GPa, ≈6.5 wt% water in the liquid) were the closest to the conditions in crystallising granite bodies and in migmatites during partial melting. From the extrapolations in Tables 5 and 6, we first draw the general conclusion that Ostwald ripening cannot have any significant effect in systems in which the mean grain size of quartz is in the range 1–10 mm as in many granites and migmatites (we emphasise that we are only discussing the effects of Ostwald ripening and that we do not consider independent effects such as the feeding of pre-existing quartz grains because of cooling or of the advection of a quartz-supersaturated liquid): quartz grain sizes in the range 1–10 mm can neither result from Ostwald ripening nor be significantly affected by Ostwald ripening, even over time scales of 10^6–10^7 years. Accordingly, Ostwald ripening of quartz should not result in an increased permeability of partially molten crustal protoliths or in an increased settling velocity of quartz in partially crystallised granitic magmas.

Table 6 Three-dimensional mean grain sizes (μm) extrapolated from our experimental data to long times, assuming a logarithmic law in time (Table 4). The error as a result of extrapolation is given in parentheses

	I	II	III	IV
$\bar{d}_0$[a]	≈2.5	≈2.1	≈5	≈1
1 a	9.7 (0.7)	7.6 (0.1)	30.3 (2.6)	5.1 (0.2)
100 a	13.3 (1.1)	10.2 (0.2)	42.3 (3.7)	7.3 (0.4)
10,000 a	16.8 (1.5)	12.9 (0.3)	54.3 (4.9)	9.6 (0.5)
1 Ma	20.4 (1.9)	15.6 (0.4)	66.3 (6.2)	11.9 (0.7)

[a]Estimated initial 3-D mean grain sizes

The effect of Ostwald ripening on the nucleation densities of crystals in magmas

Finally, we want to point to a situation where the role of Ostwald ripening could be more important, namely during the nucleation of quartz in a magma chamber. An important aspect of Ostwald ripening is that an increase in $\bar{d}$ by a factor f is associated with a decrease in the number density of grains, N_v, by a factor of the order of f^3. For simplicity, we assume that the grains have all the same shape and the same size d. The volume fraction of solid grains is equal to $N_v g d^3$, where g is a numerical factor depending on the shape of the grains. If the volume fraction of grains remains constant during coarsening, then N_v is proportional to d^{-3}. Swanson (1977) made crystallization experiments with a granitic liquid (3.5 wt% H_2O) and a granodioritic liquid (6.5 wt% H_2O); he obtained large number densities, up to 10^8 cm^{-3}, of minute grains of quartz (1–10 μm in diameter according to his Fig. 4). For such a fine grain size, Ostwald ripening can result in a relatively rapid increase of the mean grain size as observed in our experiments (Fig. 6). Considering the extrapolations in Table 6 for series IV, $\bar{d}$ changes by a factor 5 in only one year: in terms of the number density of grains, this increase corresponds to a decrease of N_v by more than two orders of magnitude! Because of fine grain size of crystalline nuclei, we suggest that Ostwald ripening may be very active during or at the end of nucleation events in magmas and result in the consumption of a significant proportion of the newly formed crystals.

Ostwald ripening in the field

It would be interesting to compare the experimental results with natural examples of partial melting. It is not possible, however, to know precisely the initial grain size of quartz in the case of large-scale crustal anatexis such

as in migmatitic terranes. Partial melting at a smaller scale around intrusions of basic to intermediate magmas is potentially more appropriate to quantify the importance of Ostwald ripening: the duration of the melting event is shorter, but the initial grain size of quartz may be measured with some confidence outside the contact metamorphism aureole. For instance, Platten (1982) described the case of feldspathic quartzites that were partially melted around shallow diorite and monzonite intrusions in Appin, Scotland. Partial melting of the quartz–feldspar assemblage formed a quartz-saturated eutectic liquid that crystallised with a granophyric texture on cooling. The granophyric matrix contained equant grains of quartz that were similar in size to the recrystallised grains in the quartzite (≈0.1 mm; Platten 1982), but that developed a bipyramidal habit characteristic of quartz phenocrysts in rhyolites. According to Platten, the crystal faces formed on cooling by deposition of quartz from the melt as rim overgrowths on the residual quartz grains. The development of rim overgrowths on residual grains of quartz was also observed in a granite partially melted around a small diorite plug (Didier et al. 1987). There are two lessons to draw from these studies:

1. In the feldspathic quartzites, partial melting does not seem to result in a noticeable grain coarsening of quartz. Platten (1982) estimated the minimum contact temperatures as 780 °C and the confining pressure as 50 MPa, but he did not provide an estimation of the duration of the melting event. In their simulations of crustal anatexis, Raia and Spera (1997) computed anatexic time scales in the range 10^3 to 10^5 years for anatexic length scales of order 10^2 to 10^3 m. In Appin, the thickness of the partially molten zone is only of a few metres. By extrapolating Raia and Spera's results to length scales of 1–10 m, we obtain time scales of 0.1 to 10 years. The absence of grain coarsening of quartz in the feldspathic quartzites of Appin is in good qualitative agreement with our experimental results at 800 °C and 0.2 GPa.
2. In natural settings, mechanisms other than Ostwald ripening presumably control the evolution of grain size with time. In a textural study of migmatitic pelitic schists, Dougan (1983) observed that the number of grains of quartz and muscovite per unit volume decreased during partial melting because some grains were entirely consumed in the melt-generating reaction. From Platten's (1982) and Dougan's (1983) studies, we anticipate that the textural evolution of quartz during partial melting is strongly influenced by the complete dissolution of the smaller grains of quartz on heating and the precipitation of quartz on residual grains on cooling. As in the case of Ostwald ripening, these two processes must result in a smaller number of grains per unit volume and a larger mean grain size, but the driving force is not the minimisation of the total interfacial energy. Accordingly, field examples of partial melting may not be appropriate to estimate the kinetics of Ostwald ripening even when the initial grain size of quartz can be measured.

Conclusions

We showed that Ostwald ripening of quartz in a hydrous silicic melt is very sluggish and that, in general, it should not affect the dynamics of magmatic processes. A very interesting result is that the mean grain size of quartz in our experiments is proportional to ln t (or $t^{1/n}$ with $n = 5$–7) whereas LSW theory predicts a kinetic law in $t^{1/2}$ or $t^{1/3}$. We emphasise, however, that Ostwald ripening may follow different kinetics for other mineral species: for instance, Higgins (1998) studied the Lac-St-Jean anorthosite complex, Canada and concluded that Ostwald ripening is efficient for plagioclase and olivine; Waters and Boudreau (1996) also found that crystal size distributions of chromite grains from the Stillwater complex were significantly affected by crystal ageing. Therefore, in the future, it will be necessary to better characterise the behaviour of major silicate species (olivine, plagioclase, pyroxene, etc.) and to identify the systems in which Ostwald ripening may be important.

Acknowledgements This work was supported by the Institut National des Sciences de l'Univers. The manuscript benefited from discussions with Pierre Boivin, Bertrand Devouard, François Faure, Tahar Hammouda and Daniel Vielzeuf, and from constructive reviews by Jim Van Orman and Michael Higgins. Assistance with the electron microprobe by Michelle Veschambre was greatly appreciated. This is INSU-CNRS contribution 265.

References

Ardell AJ (1972) The effect of volume fraction on particle coarsening: theoretical considerations. Acta Metall 20:61–71

Baker DR (1991) Interdiffusion of hydrous dacitic and rhyolitic melts and the efficacy of rhyolite contamination of dacitic enclaves. Contrib Mineral Petrol 106:462–473

Baronnet A (1984) Growth kinetics of the silicates. Fortschr Mineral 62:187–232

Brailsford AD, Wynblatt P (1979) The dependence of Ostwald ripening kinetics on particle volume fraction. Acta Metall 27:489–497

Brown M, Averkin YA, McLellan EL (1995) Melt segregation in migmatites. J Geophys Res 100:15655–15679

De Hoff RT (1984) Generalized microstructural evolution by interface controlled coarsening. Acta Metall Mater 32:43–47

De Hoff RT (1991) A geometrically general theory of diffusion controlled coarsening. Acta Metall Mater 39:2349–2360

Didier J, El Mouraouah A, Fernandez A (1987) Microtextures de refusion dans le granite migmatitique du Velay autour de la diorite du Peyron près de Burzet (Ardèche, Massif Central français). CR Acad Sci Paris 304(II):1227–1232

Dougan TW (1983) Textural relations in melanosomes of selected specimens of migmatitic pelitic schists: implications for leucosome-generating processes. Contrib Mineral Petrol 83:82–98

Dowty E (1980) Crystal growth and nucleation theory and the numerical simulation of igneous crystallization. In: Hargraves RB (ed) Physics of magmatic processes. Princeton University Press, Princeton, pp 419–485

Dresen G, Wang Z, Bai Q (1996) Kinetics of grain growth in anorthite. Tectonophysics 258:251–262
Fang Z, Patterson BR, Turner ME (1991) Growth path envelope analysis of Ostwald ripening. Metall Trans 22A:19–23
Higgins MD (1998) Origin of anorthosite by textural coarsening: quantitative measurements of a natural sequence of textural development. J Petrol 39:1307–1323
Ikeda S, Nakashima S (1999) Rolling experiment with partially molten rocks: a new apparatus and some experiments on the kinetics of material transport, dissolution and crystal growth. Eur J Mineral 11:441–453
Jurewicz SR, Watson EB (1985) The distribution of partial melt in a granitic system: the application of liquid phase sintering theory. Geochim Cosmochim Acta 49:1109–1121
Kang SS, Yoon DN (1982) Kinetics of grain coarsening during sintering of Co–Cu and Fe–Cu alloys with low liquid contents. Metall Trans 13A:1405–1411
Kang TK, Yoon DN (1978) Coarsening of tungsten grains in liquid nickel–tungsten matrix. Metall Trans 9A:433–438
Karato S (1989) Grain growth kinetics in olivine aggregates. Tectonophysics 168:255–273
Lantuéjoul C (1980) On the estimation of mean values in individual analyses of particles. Microsc Acta Suppl 4:266–273
Laporte D (1994) Wetting behaviour of partial melts during crustal anatexis: the distribution of hydrous silicic melts in polycrystalline aggregates of quartz. Contrib Mineral Petrol 116:486–499
Laporte D, Provost A (1994) The equilibrium crystal shape of silicates: implications for the grain-scale distribution of partial melts. EOS 75:364
Lifshitz IM, Slyozov VV (1961) The kinetics of precipitation from supersaturated solid solution. J Phys Chem Solids 19:35–50
Marqusee JA, Ross J (1984) Theory of Ostwald ripening: competitive growth and its dependence on volume fraction. J Chem Phys 80:536–543
Ostwald W (1901) Analytisch chemie, 3rd edn. Engelmann, Leipzig
Park Y, Hanson B (1999) Experimental investigation of Ostwald ripening rates of forsterite in the haplobasaltic system. J Volcanol Geothermal Res 90:103–113
Platten IM (1982) Partial melting of feldspathic quartzite around late Caledonian minor intrusions in Appin, Scotland. Geol Mag 119:413–419
Raia F, Spera FJ (1997) Simulations of crustal anatexis: implications for the growth and differentiation of continental crust. J Geophys Res 102:22629–22648
Saltikov SA (1967) The determination of the size distribution of particles in an opaque material from a measurement of the size distribution of their sections. In: Elias H (ed) Stereology. Springer, Berlin Heidelberg New York, pp 163–173
Solomatov VS, Stevenson DJ (1993) Kinetics of crystal growth in a terrestrial magma ocean. J Geophys Res 98:5407–5418
Swanson SE (1977) Relation of nucleation and crystal-growth rate to the development of granitic textures. Am Mineral 62: 966–978
Tullis J, Yund A (1982) Grain growth kinetics of quartz and calcite aggregates. J Geol 90:301–318
Turcotte DL, Schubert G (1982) Geodynamics. Application of continuum physics to geological problems. Wiley, Chichester, pp 231–293, 381–417
Voorhees PW (1985) The theory of Ostwald ripening. J Stat Phys 38:231–252
Wagner C (1961) Theorie der Alterung von Niederschlägen durch Umlösen. Z Elektrochem 65:581–591
Waters C, Boudreau AE (1996) A reevaluation of crystal-size distributions in chromite cumulates. Am Mineral 81:1452–1459